A deterministic solution method for the coupled system of transport equations for the electrons and phonons in polar semiconductors

2004 J. Phys. A: Math. Gen. 37 1479

(http://iopscience.iop.org/0305-4470/37/5/002)

INSTITUTE OF PHYSICS PUBLISHING JOURNAL OF PHYSICS A: MATHEMATICAL AND GENERAL

J. Phys. A: Math. Gen. **37** (2004) 1479–1497 PII: S0305-4470(04)67103-4

A deterministic solution method for the coupled system of transport equations for the electrons and phonons in polar semiconductors

M Galler and F Schürrer

Institut für Theoretische Physik, Technische Universität Graz, Petersgasse 16, A-8010 Graz, Austria

E-mail: galler@itp.tu-graz.ac.at and schuerrer@itp.tu-graz.ac.at

Received 1 August 2003
Published 19 January 2004
Online at stacks.iop.org/JPhysA/37/1479 (DOI: 10.1088/0305-4470/37/5/002)

Abstract

We present a multigroup model of the Boltzmann equations governing the transient transport regime in polar semiconductors. Efforts have been made to give an accurate description of the coupled hot-electron hot-phonon system, which allows us to study the modifications of the carrier and longitudinal optical phonon distribution functions in comparison to the usual equilibrium phonon calculations. Computations are performed for InP, taking into account all the relevant scattering mechanisms. We investigate the response of the coupled electron–phonon system to a step-like high dc electric field pulse. Moreover, we discuss the relation between our model and a matrix method.

PACS numbers: 05.60.−k, 05.20.Dd, 72.10.Dd

1. Introduction

Very large scale integration is the forthcoming design in semiconductor technology. This implies that in modern integrated electron devices, the scale length of individual components becomes comparable with the distance between successive carrier interactions with the crystal, and the well-established drift–diffusion models describing carrier transport lose their accuracy [1]. Consequently, to cope with high-field and sub-micrometre phenomena, Boltzmann transport equations (BTEs) must be applied [2]. In femtosecond laser experiments, non-equilibrium longitudinal-optical (LO) phonons have been found to strongly affect the electron distribution function. Thus, for a unified treatment, one also has to include kinetic equations for the evolution of phonons in a realistic description [3, 4].

Instead of a purely microscopic approach by means of the expensive Monte Carlo (MC) methods, we intend to introduce a multigroup model for investigating the dynamics of the electron distribution function (EDF) and LO phonon distribution function (PDF) that acts at

a mesoscopic level. The development of such deterministic solution methods for the BTEs becomes a great challenge. This is especially the case, when dealing with transient problems in semiconductors. For such investigations it is not efficient to apply MC methods, which rely on random sampling, since the results obtained can be noisy.

Based on the increasing power of modern computers, an alternative approach to the MC method was proposed by Fatemi and Odeh [5]. They developed an upwind finite-difference approximation for the Boltzmann–Poisson (BP) system. Majorana and Pidatella [6] solved the BP system with the help of a box method in the energy and angle variables and combined this approach with a classical discretization technique for advection equations based on upwinding in the spatial variable. Recently, Carrillo *et al* [7] succeeded in introducing a deterministic high-order finite-difference WENO solver for the solution of the one-dimensional BP system for semiconductor devices. In addition, other deterministic approaches, based on series expansion methods for the BTE, have been derived by Ringhofer [8]. The Galerkin method used leads to a hyperbolic system solved by finite-difference methods in space-time variables [9, 10].

In this paper we couple the electron BTE with a Boltzmann equation for phonons by taking into account the relevant quantum statistics. Furthermore, we include several valleys in the wave vector space of electrons in our model. In contrast to the above mentioned papers, our approach to discretizing the BTEs is motivated on physical grounds. We divide the wave vector spaces of electrons and phonons into small cells and transform the full BTEs into a system of coupled transport equations balancing the particle transfer among these cells. The particle density within each cell is represented by a Dirac distribution, which allows us to analytically perform the collision integrals. From a mathematical point of view, our approach is based on the method of weighted residuals [11], which is a finite-element technique.

Several variations of multigroup approaches have been published for an approximative description of the dynamics of rarefied gases. Hence, the multigroup method can be regarded as well established in the classical kinetic theory [12–14]. In this paper, we adapt this formalism to the special requirements, related to the BTE in a polar semiconductor. In such materials, the polar optical (POP) interaction between electrons and LO phonons is the main relaxation mechanism at room temperature. As a consequence, the disturbance of the PDF from thermal equilibrium, which cannot be neglected for sufficiently high doping concentrations, significantly affects the EDF. Therefore, our calculations are performed for the coupled hot-electron hot-phonon BTE system. This procedure allows us to study the modifications of the main transport properties in III–V semiconductor compounds due to non-equilibrium LO phonons. Moreover, we compare the results for the coupled system with those gained with the help of the usual assumption of LO phonons being in equilibrium.

The numerical method presented is used for the investigation of the transient transport regime in InP in response to the onset of a step-like high dc electric field. It turns out that our method exceeds the accuracy of classical drift diffusion models especially at high electric fields and when taking into account non-equilibrium LO phonons. However, it is by no means as time consuming as a typical MC method. Moreover, the simple numerical evaluation of the non-linear collision terms is responsible for a large amount of computational power saved in comparison to another mesoscopic method [4] we refer to by discussing the relations of the gained results. Therefore, our multigroup method seems to be a very powerful tool for an accurate simulation of transport phenomena influenced by hot-phonon hot-electron interactions. This approach can easily be extended to BP systems without changing the main ideas of our model.

Our paper is organized as follows: the underlying physical model for InP is described in section 2. Section 3 deals with the mathematical formulation of our multigroup model.

Finally, we apply this method to InP in section 4 and compare the results with those of the matrix method in [4].

2. The physical model

In this paper we consider n-type InP with a doping concentration of $N_D = 10^{17}\,\mathrm{cm}^{-3}$ at temperature $T_L = 300$ K. Therefore, we are allowed to neglect holes in the valence band. The conduction band is approximated by the Γ valley centred at $\langle 0, 0, 0\rangle$ and four equivalent L valleys along $\langle 1, 1, 1\rangle$. These valleys are assumed to be spherical and non-parabolic. The X valleys are neglected in our calculations.

Regarding the collision mechanisms, we consider acoustic deformation potential (ADP) and acoustic piezoelectric (PZ) scattering, polar optical (POP), optical deformation potential (ODP) scattering in L valleys and impurity scattering (IMP), which are all intravalley processes, and non-polar optical intervalley (IV) scattering. Since ADP and PZ scattering are not efficient at 300 K, these mechanisms are regarded as being elastic. For the intervalley transfer, we take into account two types of zone-boundary phonons. The ionized impurity scattering is described with the help of the Brook–Herring model and by assuming equal electron and donor concentrations. The material parameters we use in our calculations are found in table 1.

3. The multigroup approach

In this section, we present the multigroup model BTEs describing the transport properties in polar semiconductors. To begin with, we summarize below some relations needed.

The dispersion law, which relates the energy E^ν of an electron, measured from the bottom of the valley ν, with its wave vector $\boldsymbol{k}$, is given by

$$E^\nu(\boldsymbol{k})(1 + \alpha_\nu E^\nu(\boldsymbol{k})) = \frac{\hbar^2 k^2}{2m_\nu^*} \tag{1}$$

and vice versa, $k^\nu(E) = \frac{1}{\hbar}[2m_\nu^* E(1 + \alpha_\nu E)]^{\frac{1}{2}}$. Here, k denotes the modulus of the wave vector, α_ν and m_ν^* are, respectively, the non-parabolicity factor and the effective mass in the valley ν. This implies that the density of states $Z^\nu(E) = m_\nu^*(2\pi\hbar)^{-3}(1 + 2\alpha_\nu E)[2m_\nu^* E(1 + \alpha_\nu E)]^{\frac{1}{2}}$.

As for phonons, we apply the standard approximations for the energy–momentum rule, i.e. the energy $\hbar\omega(\boldsymbol{q})$ and the wave vector $\boldsymbol{q}$ are related via $\omega_{ac}(\boldsymbol{q}) = v_s|\boldsymbol{q}|$ and $\omega_{op}(\boldsymbol{q}) = \omega_0$ in the cases of acoustic and optical phonons, respectively. The symbol v_s denotes the sound velocity.

The wave vectors $\boldsymbol{k}$ and $\boldsymbol{q}$ are represented as $\boldsymbol{k} = (k\sin\alpha\cos\varphi, k\sin\alpha\sin\varphi, k\cos\alpha)$ and $\boldsymbol{q} = (q\sin\beta\cos\epsilon, q\sin\beta\sin\epsilon, q\cos\beta)$ in a coordinate system whose z-axis is parallel to the direction of the external electric field $\boldsymbol{E}$. Figure 1 explains the meaning of the angles used. It illustrates a scattering event from an electron state $\boldsymbol{k}$ to $\boldsymbol{k}'$, absorbing a phonon with wave vector $\boldsymbol{q}$. For our purposes, it is convenient to introduce the quantities $\vartheta = \cos\alpha$ and $\chi = \cos\beta$.

Due to the cylindrical symmetry with respect to the electric field $\boldsymbol{E}$, the electron distribution function $f^\nu(\boldsymbol{k})$ in the valley ν and the LO phonon distribution function $g(\boldsymbol{q})$ do not depend on the azimuthal angles φ and ϵ. In other words, we consider $f^\nu = f^\nu(E, \vartheta)$ and $g = g(q, \chi)$. In the EDF, we use the electron energy E as one of the independent variables instead of the modulus of the wave vector k for convenience.

Table 1. Material parameters used in InP.

General characteristics					
Quantity	Symbol	Unit	Value		
Mass density	ρ	kg m^{-3}	4830		
Sound velocity	v_s	m s^{-1}	5160		
HF relative dielectric constant	κ_∞		9.56		
Static relative dielectric constant	κ_0		12.3		
LO phonon relaxation time	τ_L	ps	5.8		
Band parameters					
Quantity	Symbol	Unit	Valley Γ	Valley L	
Relative effective mass	m^*/m_0		0.08	0.4	
Non-parabolicity factor	α^*	(eV)$^{-1}$	0.627	0.621	
Gap referred to Γ minimum	$\Delta_{\nu\mu}$	eV		0.610	
Number of equivalent valleys	$\mathcal{Z}_\mu$		1	4	
Intravalley scattering parameters					
Quantity	Symbol	Unit	Valley Γ	Valley L	
Acoustic deformation potential	D_A	eV m^{-1}	7	12	
Piezoelectric constant	D_{PZ}	C m^{-2}	0.0131	0.0131	
TO phonons					
Deformation potential	D_{TO}	eV m^{-1}		6.7×10^{10}	
Energy	$\hbar\omega_{TO}$	meV		43	
LO phonons					
Energy	$\hbar\omega_{LO}$	meV	43.20	43.20	
Intervalley scattering parameters (intervalley phonon 1)					
	Energy $\hbar\omega_{\nu\mu}$ (meV)			Deformation potential $D_{\nu\mu}$ (10^9 eV m^{-1})	
	Γ	L		Γ	L
Γ		33.7	Γ		137
L	33.7	33.7	L	137	56
Intervalley scattering parameters (intervalley phonon 2)					
	Energy $\hbar\omega_{\nu\mu}$ (meV)			Deformation potential $D_{\nu\mu}$ (10^9 eV m^{-1})	
	Γ	L		Γ	L
Γ		6.8	Γ		14
L	6.8		L	14	

3.1. The electron Boltzmann equation

The evolution of the electron distribution function f^ν in bulk semiconductors is governed by the electron BTE

$$\frac{\partial f^\nu}{\partial t} - \frac{e}{\hbar}\boldsymbol{E}\cdot\nabla_{\boldsymbol{k}} f^\nu = \sum_\xi C_\xi[f^\nu]. \tag{2}$$

In this equation, ξ represents all the involved scattering mechanisms, mentioned in section 2. The collision terms $C_\xi[f^\nu]$ typically read, neglecting degeneracy,

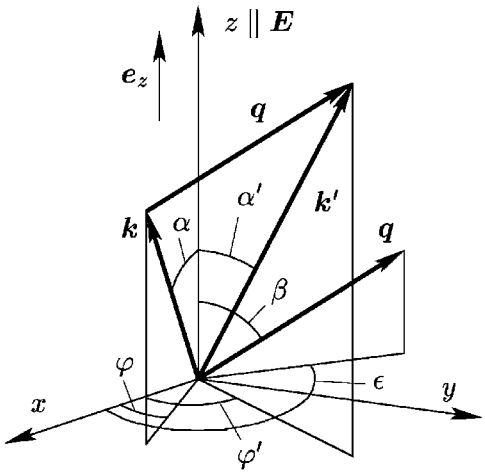

Figure 1. The absorption of a phonon with wave vector $\boldsymbol{q}$, scattering an electron from the initial state $\boldsymbol{k}$ to the final state $\boldsymbol{k}'$.

Table 2. Transition rates.

Electrons	
Scattering type ξ	$S_\xi(\boldsymbol{k} \to \boldsymbol{k}')$
ADP scattering	$2\pi D_{\mathrm{A}}^2 g^{\mathrm{ac}}(\lvert\boldsymbol{k}-\boldsymbol{k}'\rvert)\lvert\boldsymbol{k}-\boldsymbol{k}'\rvert\delta[E(\boldsymbol{k}')-E(\boldsymbol{k})]/v_{\mathrm{s}}\rho V$
PZ scattering	$2\pi(eD_{\mathrm{PZ}})^2 g^{\mathrm{ac}}(\lvert\boldsymbol{k}-\boldsymbol{k}'\rvert)\delta[E(\boldsymbol{k}')-E(\boldsymbol{k})]/(\kappa_0\epsilon_0)^2 v_{\mathrm{s}}\rho V\lvert\boldsymbol{k}-\boldsymbol{k}'\rvert$
POP scattering	$K_{\mathrm{POP}} := \pi e^2\omega_{\mathrm{LO}}(1/\kappa_\infty - 1/\kappa_0)/\epsilon_0 V$
Emission	$K_{\mathrm{POP}}[g^{\mathrm{LO}}(\boldsymbol{k}-\boldsymbol{k}')+1]\delta[E(\boldsymbol{k}')-E(\boldsymbol{k})+\hbar\omega_{\mathrm{LO}}]/\lvert\boldsymbol{k}-\boldsymbol{k}'\rvert^2$
Absorption	$K_{\mathrm{POP}} g^{\mathrm{LO}}(\boldsymbol{k}'-\boldsymbol{k})\delta[E(\boldsymbol{k}')-E(\boldsymbol{k})-\hbar\omega_{\mathrm{LO}}]/\lvert\boldsymbol{k}-\boldsymbol{k}'\rvert^2$
ODP scattering	
Emission	$\pi D_{\mathrm{TO}}^2[g^{\mathrm{TO}}(\boldsymbol{k}-\boldsymbol{k}')+1]\delta[E(\boldsymbol{k}')-E(\boldsymbol{k})+\hbar\omega_{\mathrm{TO}}]/\omega_{\mathrm{TO}}\rho V$
Absorption	$\pi D_{\mathrm{TO}}^2 g^{\mathrm{TO}}(\boldsymbol{k}'-\boldsymbol{k})\delta[E(\boldsymbol{k}')-E(\boldsymbol{k})-\hbar\omega_{\mathrm{TO}}]/\omega_{\mathrm{TO}}\rho V$
IMP scattering	$2\pi N_{\mathrm{D}} e^4\delta[E(\boldsymbol{k}')-E(\boldsymbol{k})]/\hbar\kappa_0^2\epsilon_0^2 V\left[4k^2\sin^2\left(\boldsymbol{k}\cdot\boldsymbol{k}'/2kk'\right)+1/L_{\mathrm{D}}^2\right]^2$
IV scattering	
Emission	$\pi\mathcal{Z}_\mu D_{\nu\mu}^2[g^{\mathrm{IV}}(\boldsymbol{k}-\boldsymbol{k}')+1]\delta[E^\mu(\boldsymbol{k}')-E^\nu(\boldsymbol{k})+\hbar\omega_{\nu\mu}-\Delta_{\nu\mu}]/\omega_{\nu\mu}\rho V$
Absorption	$\pi\mathcal{Z}_\mu D_{\nu\mu}^2 g^{\mathrm{IV}}(\boldsymbol{k}'-\boldsymbol{k})\delta[E^\mu(\boldsymbol{k}')-E^\nu(\boldsymbol{k})-\hbar\omega_{\nu\mu}-\Delta_{\nu\mu}]/\omega_{\nu\mu}\rho V$
LO phonons	
Scattering type η	$S_\eta(\boldsymbol{q})$
POP scattering	
Emission	$K_{\mathrm{POP}} f^\nu(\boldsymbol{k})\delta[E(\boldsymbol{k}-\boldsymbol{q})-E(\boldsymbol{k})+\hbar\omega_{\mathrm{LO}}]/\lvert\boldsymbol{q}\rvert^2$
Absorption	$K_{\mathrm{POP}} f^\nu(\boldsymbol{k})\delta[E(\boldsymbol{k}+\boldsymbol{q})-E(\boldsymbol{k})-\hbar\omega_{\mathrm{LO}}]/\lvert\boldsymbol{q}\rvert^2$

$$C_\xi[f^\nu] = \frac{V}{8\pi^3}\int \mathrm{d}^3k'[S_\xi(\boldsymbol{k}'\to\boldsymbol{k})f^\nu(\boldsymbol{k}') - S_\xi(\boldsymbol{k}\to\boldsymbol{k}')f^\nu(\boldsymbol{k})]. \tag{3}$$

The symbol $S_\xi(\boldsymbol{k}\to\boldsymbol{k}')$ is the transition rate from state $\boldsymbol{k}$ to $\boldsymbol{k}'$, V is the volume of the crystal and e denotes elementary charge. Here and in all the other integrals with unspecified integration intervals, the integration is performed over all the states $\boldsymbol{k}$ associated with the valley ν. A list of the expressions used for the transition rates S_ξ [15, 16] is given in table 2. For ODP and IV scattering, the phonon distribution functions g^{TO} and g^{IV} are assumed to be the equilibrium Bose–Einstein distributions. In the cases of ADP and PZ scattering with

acoustic phonons, equipartition is regarded: $g^{\mathrm{ac}}(\boldsymbol{q}) \approx g^{\mathrm{ac}}(\boldsymbol{q}) + 1 \approx k_{\mathrm{B}} T_{\mathrm{L}}/\hbar\omega_{\mathrm{ac}}(\boldsymbol{q})$, where k_{B} is the Boltzmann constant.

To deal with the electron BTE, we proceed as follows. First, we introduce the new function F^ν, defined by $F^\nu(E,\vartheta) = Z^\nu(E) f^\nu(E,\vartheta)$. As a consequence, the integration of the EDF with respect to $\boldsymbol{k}$ can be written as

$$\frac{1}{8\pi^3}\int \mathrm{d}^3k f^\nu(\boldsymbol{k}) = \int \mathrm{d}E \int \mathrm{d}\vartheta \int_0^{2\pi} \mathrm{d}\varphi F^\nu(E,\vartheta). \tag{4}$$

The second step of constructing the multigroup model BTEs consists of introducing a partition of the (E,ϑ) space into cells $\mathcal{C}_{ij}^\nu = \left[\mathcal{E}_{i-1}^\nu, \mathcal{E}_i^\nu\right] \times \left[\Theta_{j-1}^\nu, \Theta_j^\nu\right]$, $i = 1, 2, \ldots, N^\nu$, $j = 1, 2, \ldots, M^\nu$. The boundary values of this partition are set to $\Theta_0^\nu = -1$, $\Theta_{M^\nu}^\nu = 1$, $\mathcal{E}_0^\nu = 0$ and $\mathcal{E}_{N^\nu}^\nu = E_{\max}$, so that $F^\nu(E_{\max},\vartheta)$ can be considered negligible.

To obtain an approximative solution to the electron BTE, we express the distribution function F^ν as the finite sum

$$F^\nu(E,\vartheta) = \sum_{i=1}^{N^\nu}\sum_{j=1}^{M^\nu} n_{ij}^\nu \delta\left(E - E_i^\nu\right)\delta\left(\vartheta - \vartheta_j^\nu\right). \tag{5}$$

The poles of the Dirac distributions must fulfil the conditions $E_i^\nu \in I_i^{\mathcal{E},\nu} = \left(\mathcal{E}_{i-1}^\nu, \mathcal{E}_i^\nu\right)$ and $\vartheta_j^\nu \in I_j^{\Theta,\nu} = \left(\Theta_{j-1}^\nu, \Theta_j^\nu\right)$. For a physical interpretation of the coefficients n_{ij}^ν in (5), we evaluate the particle density $\langle n^\nu\rangle_{ij}$, due to electrons with energies and directions within the cell $\mathcal{C}_{ij}^\nu$ in the valley ν. Following the definitional equation of this quantity and replacing the original EDP by the ansatz made above, we find by taking advantage of (4)

$$\left\langle n_{ij}^\nu\right\rangle = \frac{1}{4\pi^3}\int_{\mathcal{C}_{ij}^\nu} \mathrm{d}^3k f^\nu(\boldsymbol{k}) = 4\pi \sum_{a=1}^{N^\nu}\sum_{b=1}^{M^\nu}\int_{I_i^{\mathcal{E},\nu}} \mathrm{d}E \int_{I_i^{\Theta,\nu}} \mathrm{d}\vartheta\, n_{ab}^\nu \delta\left(E - E_a^\nu\right)\delta\left(\vartheta - \vartheta_b^\nu\right) = 4\pi n_{ij}^\nu. \tag{6}$$

In other words, the coefficients n_{ij}^ν are equal to the electron density in the cell $\mathcal{C}_{ij}^\nu$ except for a constant factor. The same procedure allows us to determine other important macroscopic quantities such as the total electron density $\langle n^\nu\rangle$, the drift velocity $\langle v^\nu\rangle$ in the direction of the electric field (unit vector $\boldsymbol{e}_z$) and the mean energy $\langle E^\nu\rangle$:

$$\langle n^\nu\rangle = \frac{1}{4\pi^3}\int \mathrm{d}^3k f^\nu(\boldsymbol{k}) = 4\pi \sum_{i=1}^{N^\nu}\sum_{j=1}^{M^\nu} n_{ij}^\nu \tag{7a}$$

$$\langle n^\nu\rangle\langle v^\nu\rangle = \frac{1}{4\pi^3\hbar}\int \mathrm{d}^3k \frac{\partial E(\boldsymbol{k})}{\partial \boldsymbol{k}}\cdot \boldsymbol{e}_z f^\nu(\boldsymbol{k}) = \frac{4\pi\hbar}{m_\nu^*}\sum_{i=1}^{N^\nu}\sum_{j=1}^{M^\nu}\frac{k^\nu\left(E_i^\nu\right)}{1+2\alpha_\nu E_i^\nu}\vartheta_j^\nu n_{ij}^\nu \tag{7b}$$

$$\langle n^\nu\rangle\langle E^\nu\rangle = \frac{1}{4\pi^3}\int \mathrm{d}^3k E^\nu(\boldsymbol{k}) f^\nu(\boldsymbol{k}) = 4\pi \sum_{i=1}^{N^\nu}\sum_{j=1}^{M^\nu} E_i^\nu n_{ij}^\nu. \tag{7c}$$

To construct the equations which govern the evolution of the coefficients n_{ij}^ν, we follow the method of weighted residuals [11]. The electron BTE (2) is integrated over the cell $\mathcal{C}_{ij}^\nu$. With the help of (4), the integration variables are transformed into E and ϑ. Whenever the product $Z^\nu f^\nu$ appears, it is replaced by the ansatz (5). This procedure ends in a set of $N^\nu \times M^\nu$ equations for the $N^\nu \times M^\nu$ unknowns n_{ij}^ν.

Following this strategy, we find for the first term of the electron BTE, containing the temporal derivative,

$$\frac{1}{8\pi^3}\int_{\mathcal{C}_{ij}^{\nu}} \mathrm{d}^3k \frac{\partial f^{\nu}}{\partial t} = 2\pi \frac{\partial n_{ij}^{\nu}}{\partial t}. \tag{8}$$

Special attention is paid to a suitable formulation of the force term $C_{\boldsymbol{E}}[f^{\nu}] = -e\boldsymbol{E}\cdot\nabla_{\boldsymbol{k}} f^{\nu}/\hbar$. Here, our procedure yields, without writing terms that contain the azimuthal angle φ since these terms vanish after the integration with respect to φ,

$$\begin{aligned}\frac{1}{8\pi^3}\int_{\mathcal{C}_{ij}^{\nu}} \mathrm{d}^3k C_{\boldsymbol{E}}[f^{\nu}] &= \frac{-e|\boldsymbol{E}|}{8\pi^3\hbar}\int_{\mathcal{C}_{ij}^{\nu}} \mathrm{d}^3k \left(\vartheta\frac{\partial f^{\nu}}{\partial k} + \frac{1-\vartheta^2}{k}\frac{\partial f^{\nu}}{\partial \vartheta}\right)\\ &= -\frac{2\pi e|\boldsymbol{E}|}{\hbar}\sum_{a=1}^{N^{\nu}}\sum_{b=1}^{M^{\nu}}\int_{I_i^{\mathcal{E},\nu}} \mathrm{d}E \int_{I_j^{\Theta,\nu}} \mathrm{d}\vartheta\\ &\quad\times\left[\left(\frac{\partial k^{\nu}(E)}{\partial E}\right)^{-1}\vartheta n_{ab}^{\nu}\delta\big(\vartheta-\vartheta_b^{\nu}\big)\frac{\partial}{\partial E}\delta\big(E-E_a^{\nu}\big)\right.\\ &\quad\left.+\frac{1-\vartheta^2}{k^{\nu}(E)}n_{ab}^{\nu}\delta\big(E-E_a^{\nu}\big)\frac{\partial}{\partial\vartheta}\delta\big(\vartheta-\vartheta_b^{\nu}\big)\right].\end{aligned} \tag{9}$$

The application of the standard algebra for evaluating the derivatives of Dirac distributions to this result leads to

$$\begin{aligned}\frac{1}{8\pi^3}\int_{\mathcal{C}_{ij}^{\nu}} \mathrm{d}^3k C_{\boldsymbol{E}}[f^{\nu}] &= \frac{2\pi e|\boldsymbol{E}|}{\hbar}\left\{\vartheta_j^{\nu}\int_{I_i^{\mathcal{E},\nu}} \mathrm{d}E\,\delta\big(E-E_i^{\nu}\big)\frac{\hbar^2}{m_{\nu}^*}\frac{\partial}{\partial E}\left(\frac{k^{\nu}(E)}{1+2\alpha_{\nu}E}n_{ij}^{\nu}\right)\right.\\ &\quad\left.+\frac{1}{k^{\nu}\big(E_i^{\nu}\big)}\int_{I_j^{\Theta,\nu}}\mathrm{d}\vartheta\,\delta\big(\vartheta-\vartheta_j^{\nu}\big)\frac{\partial}{\partial\vartheta}\big[(1-\vartheta^2)n_{ij}^{\nu}\big]\right\}.\end{aligned} \tag{10}$$

Now, we replace the derivatives with respect to E and ϑ by

$$\frac{\partial}{\partial E}\left(\frac{k^{\nu}(E)}{1+2\alpha_{\nu}E}n_{ij}^{\nu}\right) = -\frac{1}{\mathcal{E}_i^{\nu}-\mathcal{E}_{i-1}^{\nu}}\left[\frac{k^{\nu}\big(\mathcal{E}_i^{\nu}\big)}{1+2\alpha_{\nu}\mathcal{E}_i^{\nu}}\big[n_{ij}^{\nu}\big]^{+} - \frac{k^{\nu}\big(\mathcal{E}_{i-1}^{\nu}\big)}{1+2\alpha_{\nu}\mathcal{E}_{i-1}^{\nu}}\big[n_{ij}^{\nu}\big]^{-}\right] \tag{11a}$$

$$\frac{\partial}{\partial\vartheta}\big[(1-\vartheta^2)n_{ij}^{\nu}\big] = -\frac{1}{\Theta_j^{\nu}-\Theta_{j-1}^{\nu}}\big[\big(1-\Theta_j^{\nu 2}\big)n_{i,j+1}^{\nu} - \big(1-\Theta_{j-1}^{\nu 2}\big)n_{ij}^{\nu}\big] \tag{11b}$$

with

$$\big[n_{ij}^{\nu}\big]^{+} = \begin{cases} n_{i+1,j}^{\nu} & \text{if} \quad \vartheta_j^{\nu} > 0\\ n_{ij}^{\nu} & \text{if} \quad \vartheta_j^{\nu} < 0\end{cases} \qquad \big[n_{ij}^{\nu}\big]^{-} = \begin{cases} n_{ij}^{\nu} & \text{if} \quad \vartheta_j^{\nu} > 0\\ n_{i-1,j}^{\nu} & \text{if} \quad \vartheta_j^{\nu} < 0.\end{cases}$$

These expressions are justified by heuristically gained evolution equations for the particle density $\langle n_{ij}^{\nu}\rangle$ in the cell $\mathcal{C}_{ij}^{\nu}$. The detailed derivation of these expressions, which is based on the pseudo-Newtonian law for the electron state $\hbar\dot{\boldsymbol{k}} = -e\boldsymbol{E}$, is found in [17].

As a result, we obtain the multigroup version of the force term by inserting (3.1) into (10):

$$\begin{aligned}\frac{1}{8\pi^3}\int_{\mathcal{C}_{ij}^{\nu}} \mathrm{d}^3k C_{\boldsymbol{E}}[f^{\nu}] &= -\frac{2\pi e|\boldsymbol{E}|}{\hbar}\left\{\frac{\hbar^2}{m_{\nu}^*}\frac{\vartheta_j^{\nu}}{\mathcal{E}_i^{\nu}-\mathcal{E}_{i-1}^{\nu}}\left[\frac{k^{\nu}\big(\mathcal{E}_i^{\nu}\big)}{1+2\alpha_{\nu}\mathcal{E}_i^{\nu}}\big[n_{ij}^{\nu}\big]^{+} - \frac{k^{\nu}\big(\mathcal{E}_{i-1}^{\nu}\big)}{1+2\alpha_{\nu}\mathcal{E}_{i-1}^{\nu}}\big[n_{ij}^{\nu}\big]^{-}\right]\right.\\ &\quad\left.+\frac{1}{k^{\nu}\big(E_i^{\nu}\big)}\frac{1}{\Theta_j^{\nu}-\Theta_{j-1}^{\nu}}\big[\big(1-\Theta_j^{\nu 2}\big)n_{ij+1}^{\nu} - \big(1-\Theta_{j-1}^{\nu 2}\big)n_{ij}^{\nu}\big]\right\}.\end{aligned} \tag{12}$$

From a physical point of view, expression (13) describes the fluxes between neighbouring cells induced by the electric field. The particle conservation with respect to the electric field can be ensured, when terms which describe flows at boundary cells in and out of the chosen finite (E, ϑ) space are set to zero.

Now, we turn to the collision terms. As for generality, we consider a scattering mechanism ξ acting between the valleys ν and μ. With this formalism, we can describe all the scattering mechanisms ($\mu = \nu$ for intravalley scattering) except for the POP interaction (section 3.3).

Firstly, the loss terms $L_\xi[f^\nu] = f^\nu(\boldsymbol{k})V \int \mathrm{d}^3k' S_\xi^{\nu\to\mu}(\boldsymbol{k} \to \boldsymbol{k}')/8\pi^3$ for the valley ν (see (3)) are transformed into our multigroup scheme:

$$\frac{1}{8\pi^3}\int_{\mathcal{C}_{ij}^\nu} \mathrm{d}^3k L_\xi[f^\nu] = 2\pi \sum_{a=1}^{N^\mu}\sum_{b=1}^{M^\mu} \left\langle S_{\xi,ab}^{\nu\to\mu}\right\rangle_{ij} n_{ij}^\nu \tag{13}$$

with

$$\left\langle S_{\xi,ab}^{\mu\to\nu}\right\rangle_{ij} = \frac{V}{8\pi^3}\int_{I_i^{\mathcal{E},\nu}} \mathrm{d}E \int_{I_j^{\Theta,\nu}} \mathrm{d}\vartheta \int_{\mathcal{C}_{ab}^\mu} \mathrm{d}^3k' S_\xi^{\nu\to\mu}(\boldsymbol{k} \to \boldsymbol{k}')\delta\big(E - E_i^\nu\big)\delta\big(\vartheta - \vartheta_j^\nu\big). \tag{14}$$

Secondly, the gain terms $G_\xi[f^\nu] = V \int \mathrm{d}^3k' S_\xi^{\mu\to\nu}(\boldsymbol{k}' \to \boldsymbol{k}) f^\mu(\boldsymbol{k}')/8\pi^3$ are found to equal

$$\frac{1}{8\pi^3}\int_{\mathcal{C}_{ij}^\nu} \mathrm{d}^3k\, G_\xi[f^\nu] = \frac{V}{(8\pi^3)^2}\sum_{a=1}^{N^\mu}\sum_{b=1}^{M^\mu}\int_{\mathcal{C}_{ij}^\nu} \mathrm{d}^3k \int_{\mathcal{C}_{ab}^\mu} \mathrm{d}^3k' S_\xi^{\mu\to\nu}(\boldsymbol{k}' \to \boldsymbol{k}) f^\mu(\boldsymbol{k}'). \tag{15}$$

By exchanging the names of the integration variables $\boldsymbol{k}$ and $\boldsymbol{k}'$ and comparing the result with (14), it can easily be seen that

$$\frac{1}{8\pi^3}\int_{\mathcal{C}_{ij}^\nu} \mathrm{d}^3k\, G_\xi[f^\nu] = 2\pi \sum_{a=1}^{N^\mu}\sum_{b=1}^{M^\mu} \left\langle S_{\xi,ij}^{\mu\to\nu}\right\rangle_{ab} n_{ab}^\mu. \tag{16}$$

Finally, we achieve the multigroup formulation of the electron BTE for the valley ν by adding expressions (8), (12), (13) and (14). These equations read, cancelling a factor 2π and neglecting obsolete valley indices,

$$\begin{aligned}
&\frac{\partial n_{ij}^\nu}{\partial t} - \frac{e|\boldsymbol{E}|}{\hbar}\left\{\frac{\hbar^2}{m_\nu^*}\frac{\vartheta_j^\nu}{\mathcal{E}_i^\nu - \mathcal{E}_{i-1}^\nu}\left[\frac{k^\nu\big(\mathcal{E}_i^\nu\big)}{1+2\alpha_\nu\mathcal{E}_i^\nu}\big[n_{ij}^\nu\big]^+ - \frac{k^\nu\big(\mathcal{E}_{i-1}^\nu\big)}{1+2\alpha_\nu\mathcal{E}_{i-1}^\nu}\big[n_{ij}^\nu\big]^-\right]\right.\\
&\qquad\left. + \frac{1}{k^\nu\big(E_i^\nu\big)}\frac{1}{\Theta_j^\nu - \Theta_{j-1}^\nu}\big[\big(1-\big(\Theta_j^\nu\big)^2\big)n_{ij+1}^\nu - \big(1-\big(\Theta_{j-1}^\nu\big)^2\big)n_{ij}^\nu\big]\right\}\\
&\quad = \sum_{\xi,\xi\neq\mathrm{IV,POP}}\sum_{a=1}^{N^\nu}\sum_{b=1}^{M^\nu}\left(\left\langle S_{\xi,ij}^\nu\right\rangle_{ab} n_{ab}^\nu - \left\langle S_{\xi,ab}^\nu\right\rangle_{ij} n_{ij}^\nu\right) + \frac{1}{16\pi^4}\int_{\mathcal{C}_{ij}^\nu}\mathrm{d}^3k C_{\mathrm{POP}}[f^\nu]\\
&\qquad + \sum_{\mu,\mu\neq\nu}\sum_{a=1}^{N^\mu}\sum_{b=1}^{M^\mu}\left(\mathcal{Z}_\mu\left\langle S_{\mathrm{IV},ij}^{\mu\to\nu}\right\rangle_{ab} n_{ab}^\mu - \mathcal{Z}_\nu\left\langle S_{\mathrm{IV},ab}^{\nu\to\mu}\right\rangle_{ij} n_{ij}^\nu\right)
\end{aligned} \tag{17}$$

where $i = 1, 2, \ldots, N^\nu$, $j = 1, 2, \ldots, M^\nu$.

3.2. The LO phonon Boltzmann equation

The evolution equation for the distribution function $g(\boldsymbol{q})$ of LO phonons depending on the phonon state $\boldsymbol{q}$ reads

$$\frac{\partial g}{\partial t} = D_{\mathrm{PH\text{–}PH}}[g] + \sum_\nu 2\mathcal{Z}_\nu D_{\mathrm{POP}}^\nu[g]. \tag{18}$$

Here, we assume that the PDF can be disturbed by phonon–phonon thermalization processes due to $D_{\mathrm{PH-PH}}[g]$ and the POP interaction with electrons of the valleys ν according to $D^{\nu}_{\mathrm{POP}}[g]$.

The lattice scattering term in (18) is described through a relaxation time τ_{L}

$$D_{\mathrm{PH-PH}}[g] = [g_{\mathrm{L}} - g(\boldsymbol{q})]\tau_{\mathrm{L}}^{-1} \tag{19}$$

where g_{L} is the Bose–Einstein equilibrium distribution at lattice temperature T_{L}. In [3, 4], the proper choice of the parameter τ_{L} is discussed. We follow these arguments leading to the value for τ_{L} proposed in table 1.

Regarding the POP collision term, we find

$$D^{\nu}_{\mathrm{POP}}[g] = \frac{V}{8\pi^3}\int \mathrm{d}^3k\left\{S^{\mathrm{em}}_{\mathrm{POP}}(\boldsymbol{q})[g(\boldsymbol{q})+1] - S^{\mathrm{abs}}_{\mathrm{POP}}(\boldsymbol{q})g(\boldsymbol{q})\right\} \tag{20}$$

with the transition rates $S^{\mathrm{em}}_{\mathrm{POP}}(\boldsymbol{q})$ and $S^{\mathrm{abs}}_{\mathrm{POP}}(\boldsymbol{q})$ for phonon emission and absorption, respectively, which are given in table 2.

The LO phonon BTE is treated in the same way as the electron BTE. Hence, we define $G(q,\chi) = q^2 g(q,\chi)/8\pi^3$, which leads to

$$\frac{1}{8\pi^3}\int \mathrm{d}^3q\, g(\boldsymbol{q}) = \int \mathrm{d}q \int \mathrm{d}\chi \int_0^{2\pi} \mathrm{d}\epsilon\, G(q,\chi). \tag{21}$$

The wave vector space (q,χ) is divided into cells $\mathcal{D}_{xy} = [\mathcal{Q}_{x-1}, \mathcal{Q}_x] \times [\mathrm{x}_{y-1}, \mathrm{x}_y]$, $x = 1, 2, \ldots, R$, $y = 1, 2, \ldots, S$, with the boundary values $\mathrm{x}_0 = -1, \mathrm{x}_S = 1, \mathcal{Q}_0 = 0$ and $\mathcal{Q}_R = q_{\max}$. Here, $q_{\max}$ is chosen so that $g(\boldsymbol{q})$ can be considered undisturbed by the POP interaction with electrons.

Similar to (5), we represent the distribution function G by the ansatz

$$G(q,\chi) = \sum_{x=1}^{R}\sum_{y=1}^{S} r_{xy}\delta(q-q_x)\delta(\chi-\chi_y) \tag{22}$$

demanding $q_x \in I^{\mathcal{Q}}_x = (\mathcal{Q}_{x-1}, \mathcal{Q}_x)$ and $\chi_y \in I^{\mathrm{X}}_y = (\mathrm{x}_{y-1}, \mathrm{x}_y)$. Macroscopic quantities for the LO phonons can be evaluated with the help of expressions similar to those in section 3.1. As an example, the phonon density $\langle r_{xy}\rangle$ of LO phonons with wave vector $\boldsymbol{q}$ within the cell $\mathcal{D}_{xy}$ is given by

$$\langle r_{xy}\rangle = \frac{1}{8\pi^3}\int_{\mathcal{D}_{xy}} \mathrm{d}^3q\, g(\boldsymbol{q}) = 2\pi r_{xy}. \tag{23}$$

The $R \times S$ evolution equations for the coefficients r_{xy} are found by the following strategy: the phonon BTE is integrated over the cell $\mathcal{D}_{xy}$. By taking advantage of (21), we obtain an evolution equation for the function G. Here, we replace the function G by the ansatz (22) and carry out all possible integrations.

Hence, the left-hand side of the phonon BTE (18) becomes

$$\frac{1}{8\pi^3}\int_{\mathcal{D}_{xy}} \mathrm{d}^3q \frac{\partial g}{\partial t} = 2\pi\frac{\partial r_{xy}}{\partial t}. \tag{24}$$

The application of our multigroup formalism to the phonon–phonon interaction term $D_{\mathrm{PH-PH}}[g]$ yields

$$\frac{1}{8\pi^3}\int_{\mathcal{Q}_{xy}} \mathrm{d}^3q\, D_{\mathrm{PH-PH}}[g] = \frac{2\pi}{\tau_{\mathrm{L}}}\left(r^{\mathrm{equi}}_{xy} - r_{xy}\right) \tag{25}$$

where the equilibrium coefficients r^{equi}_{xy} are calculated via

$$r^{\mathrm{equi}}_{xy} = \frac{1}{16\pi^4}\int_{\mathcal{D}_{xy}} \mathrm{d}^3q \left[\exp\left(\frac{\hbar\omega_{\mathrm{LO}}}{k_{\mathrm{B}}T_{\mathrm{L}}}\right) - 1\right]^{-1}. \tag{26}$$

By summarizing the terms (24) and (25), the transformation of the phonon BTE into our multigroup scheme results in

$$\frac{\partial r_{xy}}{\partial t} = \frac{1}{\tau_{\mathrm{L}}}\left(r_{xy}^{\mathrm{equi}} - r_{xy}\right) + \sum_{\nu} \frac{2Z_\nu}{16\pi^4} \int_{\mathcal{Q}_{xy}} \mathrm{d}^3 q\, D^\nu_{\mathrm{POP}}[g] \tag{27}$$

$x = 1, 2, \ldots, R$, $y = 1, 2, \ldots, S$, except for the POP interaction term, which is discussed in the next section.

3.3. The coupling POP interaction term

In this section, we deal with the most important terms of our multigroup model—the polar optical scattering terms—that couple the electron and the LO phonon Boltzmann equations. On one hand, these expressions describe how the lattice is modified by the hot electrons. On the other, the electron transport properties are essentially influenced by these hot phonons. In consequence, these coupling terms are responsible for a significant deviation of the results from those based on the usual equilibrium phonon calculations.

To begin with, we consider the POP interaction term of the electron BTE $C_{\mathrm{POP}}[f^\nu]$. In its full form, it reads (cf table 2)

$$\begin{aligned} C_{\mathrm{POP}}[f^\nu] = \frac{V}{8\pi^3} \int \mathrm{d}^3 k' \Bigg\{ & \frac{K_{\mathrm{POP}}}{|\boldsymbol{k}-\boldsymbol{k}'|^2} f^\nu(\boldsymbol{k}')[g(\boldsymbol{k}'-\boldsymbol{k})+1]\delta[E^\nu(\boldsymbol{k}') - E^\nu(\boldsymbol{k}) - \hbar\omega_{\mathrm{LO}}] \\ & + \frac{K_{\mathrm{POP}}}{|\boldsymbol{k}-\boldsymbol{k}'|^2} f^\nu(\boldsymbol{k}') g(\boldsymbol{k}-\boldsymbol{k}')\delta[E^\nu(\boldsymbol{k}') - E^\nu(\boldsymbol{k}) + \hbar\omega_{\mathrm{LO}}] \\ & - \frac{K_{\mathrm{POP}}}{|\boldsymbol{k}-\boldsymbol{k}'|^2} f^\nu(\boldsymbol{k})[g(\boldsymbol{k}-\boldsymbol{k}')+1]\delta[E^\nu(\boldsymbol{k}') - E^\nu(\boldsymbol{k}) + \hbar\omega_{\mathrm{LO}}] \\ & - \frac{K_{\mathrm{POP}}}{|\boldsymbol{k}-\boldsymbol{k}'|^2} f^\nu(\boldsymbol{k}) g(\boldsymbol{k}'-\boldsymbol{k})\delta[E^\nu(\boldsymbol{k}') - E^\nu(\boldsymbol{k}) - \hbar\omega_{\mathrm{LO}}] \Bigg\}. \end{aligned} \tag{28}$$

Following our multigroup scheme, we integrate the electron BTE (2) over the cell $\mathcal{C}^\nu_{ij}$ and replace the distribution function by the ansatz (5). For the PDF g, we use expression (22) divided by $q^2/8\pi^3$. The additional factor 1 in the phonon emission terms is expanded to $\sum_{x'y'} V_{x'y'}\delta(q-q_{x'})\delta(\chi-\chi_{y'})/q^2$ with $V_{xy} = \left(\mathcal{Q}^3_x - \mathcal{Q}^3_{x-1}\right)(\mathrm{x}_y - \mathrm{x}_{x-1})/3$. This replacement is justified by the fact that these expressions are equal after the integration over the cell $\mathcal{D}_{xy}$:

$$\frac{1}{8\pi^3}\int_{I^{\mathcal{Q}}_x} \mathrm{d}q\, q^2 \int_{I^{\mathrm{X}}_y} \mathrm{d}\chi = \frac{1}{8\pi^3} \sum_{x'=1}^{R}\sum_{y'=1}^{S} V_{x'y'} \int_{I^{\mathcal{Q}}_x} \mathrm{d}q \int_{I^{\mathrm{X}}_y} \mathrm{d}\chi\, \delta(q-q_{x'})\delta(\chi-\chi_{y'}). \tag{29}$$

In this way, we find for the loss term $L_{\mathrm{POP}}[f^\nu]$ of the electron BTE due to POP interaction

$$\begin{aligned} & \frac{1}{8\pi^3}\int_{\mathcal{C}^\nu_{ij}} \mathrm{d}^3 k\, L_{\mathrm{POP}}[f^\nu] \\ & \qquad = 2\pi \sum_{a=1}^{N^\nu}\sum_{b=1}^{M^\nu}\sum_{x=1}^{R}\sum_{y=1}^{S} \left[\left(\left\langle \mathcal{E}^{\nu,xy}_{\mathrm{POP},ab}\right\rangle_{ij} r_{xy} + \left\langle 1^{\nu,xy}_{\mathrm{POP},ab}\right\rangle_{ij}\right) + \left\langle \mathcal{A}^{\nu,xy}_{\mathrm{POP},ab}\right\rangle_{ij} r_{xy}\right] n^\nu_{ij} \end{aligned} \tag{30}$$

with

$$\begin{aligned} \left\langle \mathcal{E}^{\nu,xy}_{\mathrm{POP},ab}\right\rangle_{ij} = \frac{V K_{\mathrm{POP}}}{q_x^3} \int_{I^{\mathcal{E},\nu}_i} \mathrm{d}E \int_{I^{\Theta,\nu}_j} \mathrm{d}\vartheta \int_{\mathcal{C}^\nu_{ab}} \mathrm{d}^3 k' \delta\left(E - E^\nu_i\right)\delta\left(\vartheta - \vartheta^\nu_j\right)\delta(|\boldsymbol{k}-\boldsymbol{k}'| - q_x) \\ \times \delta\left[(\boldsymbol{k}-\boldsymbol{k}')\cdot\boldsymbol{e}_z - q_x\chi_y\right]\delta(E^\nu(\boldsymbol{k}') - E + \hbar\omega_{\mathrm{LO}}) \end{aligned} \tag{31a}$$

$$\left\langle \mathcal{A}^{\nu,xy}_{\mathrm{POP},ab}\right\rangle_{ij} = \frac{V K_{\mathrm{POP}}}{q_x^3}\int_{I_i^{\mathcal{E},\nu}} \mathrm{d}E \int_{I_j^{\Theta,\nu}} \mathrm{d}\vartheta \int_{\mathcal{C}^{\nu}_{ab}} \mathrm{d}^3k'\, \delta\big(E - E_i^{\nu}\big)\delta\big(\vartheta - \vartheta_j^{\nu}\big)\delta(|\boldsymbol{k}' - \boldsymbol{k}| - q_x) \times \delta\left[(\boldsymbol{k}' - \boldsymbol{k})\cdot \boldsymbol{e}_z - q_x\chi_y\right]\delta(E^{\nu}(\boldsymbol{k}') - E - \hbar\omega_{\mathrm{LO}}) \tag{31b}$$

$$\left\langle 1^{\nu,xy}_{\mathrm{POP},ab}\right\rangle_{ij} = V_{xy}\left\langle \mathcal{E}^{\nu,xy}_{\mathrm{POP},ab}\right\rangle_{ij}\big/ 8\pi^3 \tag{31c}$$

and $\boldsymbol{e}_z = \boldsymbol{E}/|\boldsymbol{E}|$. With the help of similar symmetry arguments as applied in section 3.1, the multigroup version of the corresponding gain term can be deduced. Therefore, the collision term for the POP scattering of the electron BTE in our multigroup scheme is given by

$$\frac{1}{8\pi^3}\int_{\mathcal{C}^{\nu}_{ij}} \mathrm{d}^3k\, C_{\mathrm{POP}}[f^{\nu}] = 2\pi \sum_{a=1}^{N^{\nu}}\sum_{b=1}^{M^{\nu}}\sum_{x=1}^{R}\sum_{y=1}^{S}\Big[\big(\left\langle \mathcal{E}^{\nu,xy}_{\mathrm{POP},ij}\right\rangle_{ab} r_{xy} + \left\langle 1^{\nu,xy}_{\mathrm{POP},ij}\right\rangle_{ab}\big)n^{\nu}_{ab} + \left\langle \mathcal{A}^{\nu,xy}_{\mathrm{POP},ij}\right\rangle_{ab} r_{xy} n^{\nu}_{ab} - \big(\left\langle \mathcal{E}^{\nu,xy}_{\mathrm{POP},ab}\right\rangle_{ij} r_{xy} + \left\langle 1^{\nu,xy}_{\mathrm{POP},ab}\right\rangle_{ij} + \left\langle \mathcal{A}^{\nu,xy}_{\mathrm{POP},ab}\right\rangle_{ij} r_{xy}\big)n^{\nu}_{ij}\Big]. \tag{32}$$

The absorption collision coefficient $\left\langle \mathcal{A}^{\nu,xy}_{\mathrm{POP},ab}\right\rangle_{ij}$, for instance, is evaluated in the appendix.

Regarding the POP scattering term $D^{\nu}_{\mathrm{POP}}[g]$ in the phonon BTE, we find

$$D^{\nu}_{\mathrm{POP}}[g] = \frac{V}{8\pi^3}\int \mathrm{d}^3k \frac{K_{\mathrm{POP}}}{|\boldsymbol{q}|^2} f^{\nu}(\boldsymbol{k})\{[g(\boldsymbol{q}) + 1]\delta[E(\boldsymbol{k} - \boldsymbol{q}) - E(\boldsymbol{k}) + \hbar\omega_{\mathrm{LO}}] - g(\boldsymbol{q})\delta[E(\boldsymbol{k} + \boldsymbol{q}) - E(\boldsymbol{k}) - \hbar\omega_{\mathrm{LO}}]\} \tag{33}$$

by inserting the scattering rates from table 2 in (20). After performing our multigroup transformation, we obtain with the help of (5), (22) and a similar procedure for handling the additive factor 1 for phonon emission

$$\frac{1}{8\pi^3}\int_{\mathcal{D}_{xy}} \mathrm{d}^3q\, D^{\nu}_{\mathrm{POP}}[g] = 2\pi \sum_{i=1}^{N^{\nu}}\sum_{j=1}^{M^{\nu}}\Big[\big(\left\langle E^{ij}_{\mathrm{POP}}\right\rangle_{xy} - \left\langle A^{ij}_{\mathrm{POP}}\right\rangle_{xy}\big)r_{xy} + \left\langle 1^{ij}_{\mathrm{POP}}\right\rangle_{xy}\Big]n^{\nu}_{ij} \tag{34}$$

where

$$\left\langle E^{ij}_{\mathrm{POP}}\right\rangle_{xy} = \frac{V K_{\mathrm{POP}}}{8\pi^3 q_x^2}\int_{I_x^{\mathcal{Q}}} \mathrm{d}q \int_{I_y^{\mathrm{X}}} \mathrm{d}\chi \int_{\mathcal{C}^{\nu}_{ij}} \mathrm{d}^3k \frac{1}{Z^{\nu}(E^{\nu}(\boldsymbol{k}))}\delta\big(E - E_i^{\nu}\big)\delta\big(\vartheta - \vartheta_j^{\nu}\big)\delta(q - q_x) \times \delta(\chi - \chi_y)\delta[E^{\nu}(\boldsymbol{k} - \boldsymbol{q}) - E^{\nu}(\boldsymbol{k}) + \hbar\omega_{\mathrm{LO}}] \tag{35a}$$

$$\left\langle A^{ij}_{\mathrm{POP}}\right\rangle_{xy} = \frac{V K_{\mathrm{POP}}}{8\pi^3 q_x^2}\int_{I_x^{\mathcal{Q}}} \mathrm{d}q \int_{I_y^{\mathrm{X}}} \mathrm{d}\chi \int_{\mathcal{C}^{\nu}_{ij}} \mathrm{d}^3k \frac{1}{Z^{\nu}(E^{\nu}(\boldsymbol{k}))}\delta\big(E - E_i^{\nu}\big)\delta\big(\vartheta - \vartheta_j^{\nu}\big)\delta(q - q_x) \times \delta(\chi - \chi_y)\delta[E^{\nu}(\boldsymbol{k} + \boldsymbol{q}) - E^{\nu}(\boldsymbol{k}) - \hbar\omega_{\mathrm{LO}}] \tag{35b}$$

$$\left\langle 1^{ij}_{\mathrm{POP}}\right\rangle_{xy} = V_{xy}\left\langle E^{ij}_{\mathrm{POP}}\right\rangle_{xy}. \tag{35c}$$

Inserting expressions (32) and (34) in the multigroup versions of the electron and phonon equations (17) and (27), respectively, results in the final set of evolution equations for the coefficients n^{ν}_{ij} and r_{xy}.

4. Results

The application of our multigroup model to the coupled electron LO phonon regime in response to a step-like high dc electric field pulse is demonstrated in this section. All the relevant material

Table 3. The computation times t_{CPU} for the solution of the multigroup equations (17) and (27) with $N^{\Gamma} = 44$, $N^{L} = 16$, $R = 40$, $M^{\Gamma} = M^{L} = S = 12$ up to 20 ps after the onset of the electric field pulse for several electric field strengths $|\boldsymbol{E}|$ and relative accuracies ε_{r}.

	Equilibrium phonons		Hot phonons	
	$\varepsilon_{\mathrm{r}} = 10^{-3}$	$\varepsilon_{\mathrm{r}} = 10^{-5}$	$\varepsilon_{\mathrm{r}} = 10^{-3}$	$\varepsilon_{\mathrm{r}} = 10^{-5}$
$\lvert\boldsymbol{E}\rvert$ (kV cm^{-1})	t_{CPU} (s)	t_{CPU} (s)	t_{CPU} (s)	t_{CPU} (s)
1	6.1	13.6	10.7	15.8
10	9.3	16.4	11.9	19.8
50	9.8	17.9	34.2	36.3

parameters of InP are given in table 1. In our calculations, the moduli of the wave vectors of electrons and phonons are restricted up to $k_{\max} = q_{\max} = 1.7 \times 10^{9}\,\mathrm{m}^{-1}$. This implies that the maximal energies in the Γ and L valleys are $E^{\Gamma}_{\max} = 0.86\,\mathrm{eV}$ and $E^{L}_{\max} = 0.26\,\mathrm{eV}$, respectively. We assume the (E, θ) and the (q, χ) space to be equidistantly partitioned. The poles of the Dirac distributions in (5) and (22) are simply set to $E^{\nu}_{i} = \left(\mathcal{E}^{\nu}_{i} + \mathcal{E}^{\nu}_{i-1}\right)/2$, $\vartheta^{\nu}_{j} = \left(\Theta^{\nu}_{j} + \Theta^{\nu}_{j-1}\right)/2$, $q_x = (\mathcal{Q}_x + \mathcal{Q}_{x-1})/2$ and $\chi_y = (X_y + X_{y-1})/2$. Several simulations have shown that with an increasing number of intervals, the influence of this choice as well as those of the specific partitions of the (E, ϑ) and the (q, χ) space become negligible.

Before the electric field pulse begins, the electron–phonon system is supposed to be in thermal equilibrium. Therefore, the initial values of the coefficients n^{ν}_{ij} and r_{xy} are obtained from the corresponding equilibrium distributions at lattice temperature T_{L} and electron density N_{D} via (6) and (23).

The multigroup equations (17) and (27) are solved with the help of an explicit Euler scheme with adaptive step-size control demanding the relative accuracy ε_{r}. The calculations are performed with an AMD Athlon MP 2000+ processor, 1666 MHz, 2000 MB RAM. Table 3 presents the CPU times needed for integrating the multigroup equations up to 20 ps after the onset of the electric field pulse for several electric field strengths and accuracies. The partitions of the wave vector spaces in these calculations are the same as those used for deducing the current-field characteristics displayed in figure 3. The computation times increase for higher electric fields, higher required accuracies and when solving the coupled electron–phonon system instead of taking into account only equilibrium phonons. The higher demand on computational power for including hot-phonon effects in the transport model is justified by the fact that the influence of the disturbed LO phonon distribution on macroscopic transport quantities cannot be neglected in the presented case (cf figure 3). To achieve an accelerated solution technique, which is most welcome in the application to space dependent problems for a realistic device simulation, our multigroup approach can be combined with more advanced differential equation solution routines.

4.1. Validation of the method

To check the validity of the numerical procedure illustrated in the previous section, we compare the results obtained with the help of our method with those calculated by using a matrix method [4].

To this end, we study the temporal evolution of the EDF f^{Γ} of the Γ valley along the external electric field. According to the above considerations, the main quantities in our model are not the distribution function itself but the particle densities n^{ν}_{ij} of electrons with energies and polar angles within the cell $\mathcal{C}^{\nu}_{ij}$. Hence, it is not possible to compare the results of both

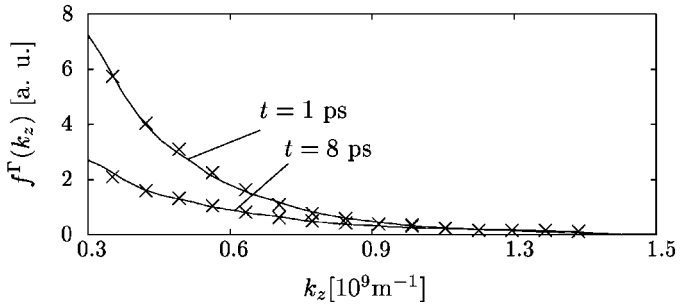

Figure 2. The electron distribution function $f^{\Gamma}(k_z)$ in the Γ valley versus the component of the wave vector k_z in the direction of the electric field with $E = 10\,\mathrm{kV\,cm^{-1}}$ for several times after the beginning of the electric field pulse. The solid lines refer to calculations performed with our multigroup approach; the crosses refer to the matrix method from Vaissiere *et al* [4].

methods directly. However, we obtain an approximate expression for the distribution function $f^{\nu}\big(k^{\nu}\big(E_i^{\nu}\big), \vartheta_j\big)$ via

$$f^{\nu}\big(k^{\nu}\big(E_i^{\nu}\big), \vartheta_j\big) = n_{ij}^{\nu}\big[Z^{\nu}\big(E_i^{\nu}\big)(\mathcal{E}_i - \mathcal{E}_{i-1})(\Theta_j - \Theta_{j-1})\big]^{-1} \tag{36}$$

which can be derived from the mean value theorem of integral calculus. It should be noted that the above approximation fails for small energies E_i^{ν} because of our equidistant energy partition. Therefore, comparisons can only be performed for sufficiently high energies.

Figure 2 displays the distribution function $f(k_z)$ versus the z-component of the wave vector in the direction of the electric field at two times after the beginning of the electric field pulse. Unfortunately, the results in [4] are given in arbitrary units, and we must introduce one scaling factor. Despite this uncertainty, figure 2 allows us to state that the results for the EDF in the Γ valley as well as its temporal evolution gained with the help of the matrix method and by our model coincide very well.

Additionally, we have evaluated the two transport parameters, the average drift velocity in the direction of the electric field and the average electron energy for several values of the applied electric field, with the help of formulae (7*b*) and (7*c*), which are reported in figure 3. Our results are compared with those of the stationary iterative method [3] and the matrix method [4]. Moreover, the results of Monte Carlo calculations [18], which are only available without hot-phonon effects for InP, are displayed in this figure. It is evident that the characteristics determined by means of our multigroup approach and the other methods mentioned agree very well in the whole range of the electric field strengths. As a consequence of the non-equilibrium-phonon-induced perturbation of the electron distribution, the electron transport parameters are significantly modified. Especially for medium electric field strengths around the threshold field at the onset of the negative differential resistivity, the values of electron drift velocity and the average energy, obtained by taking into account hot phonons, differ notably from those calculated by assuming equilibrium phonons. Hence, the consideration of hot-phonon effects is of essential importance for an accurate description of polar semiconductors with high doping concentrations.

According to the comparisons displayed in figures 2 and 3, we find that the investigation of the transient transport regime by means of our multigroup model leads to results which are equivalent to those of the matrix method presented in [4].

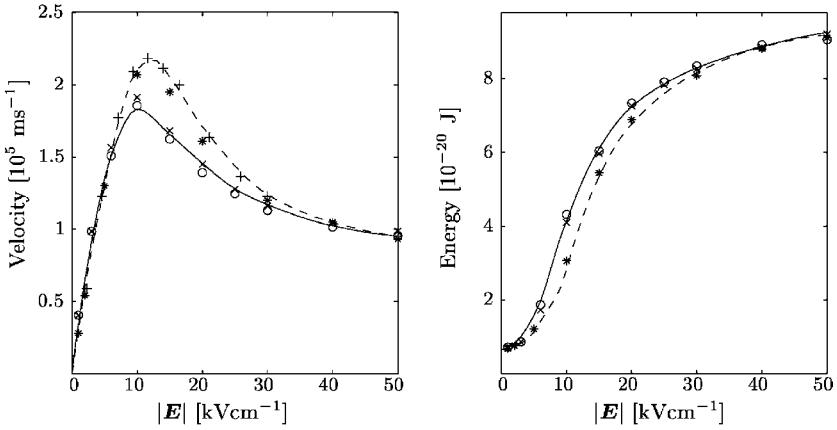

Figure 3. Average drift velocity and average electron energy as a function of the applied electric field, computed at 20 ps from the beginning of the dc field pulse: (——) presented multigroup approach for hot phonons; (- - -) presented multigroup approach for equilibrium phonons; (○) stationary iterative method [3] for hot phonons; (×) matrix method [4] for hot phonons; (∗) stationary iterative method [3] for equilibrium phonons and (+) Monte Carlo calculations [18] for equilibrium phonons.

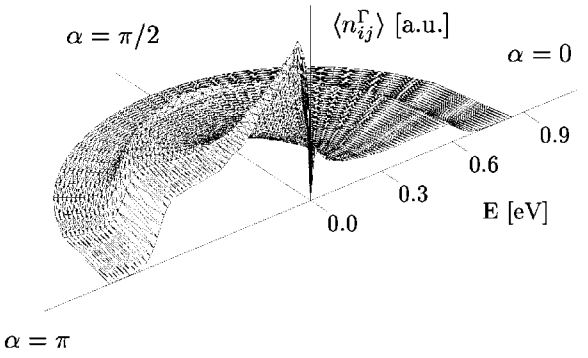

Figure 4. The electron densities $\langle n_{ij}^{\Gamma} \rangle$ in the cells $\mathcal{C}_{ij}^{\Gamma}$ in the Γ valley at $t = 8$ ps after the onset of the electric pulse with $E = 10\,\mathrm{kV\,cm^{-1}}$.

4.2. Electron distribution function

For studying the properties of the EDF in the valleys considered, we display the electron densities $\langle n_{ij}^{\nu} \rangle$ versus the cells $\mathcal{C}_{ij}^{\nu}$. Figure 4 depicts the electron densities $\langle n_{ij}^{\Gamma} \rangle$ in the cells $\mathcal{C}_{ij}^{\Gamma}$ in the Γ valley at $t = 8$ ps after the onset of the electric pulse with $E = 10\,\mathrm{kV\,cm^{-1}}$. Typically, we find a rapid decrease of the electron density at energy 0.6 eV relative to the bottom of the L valleys. Moreover, we draw attention to the strong asymmetry of the displayed particle density with respect to the electric field which reflects the low effective mass of Γ electrons. This fact allows us to argue that the classical drift diffusion models with their restriction to close to equilibrium states would hardly yield reliable results for the considered physical situation. Therefore, a mesoscopic model such as our multigroup approach is certainly a good choice for a careful investigation of this problem.

In figure 5, we display the electron densities $\langle n_{ij}^{L} \rangle$ versus the cells $\mathcal{C}_{ij}^{L}$ in the L valley, evaluated at $t = 8$ ps after the onset of the electric pulse with $E = 10\,\mathrm{kV\,cm^{-1}}$. Here, the

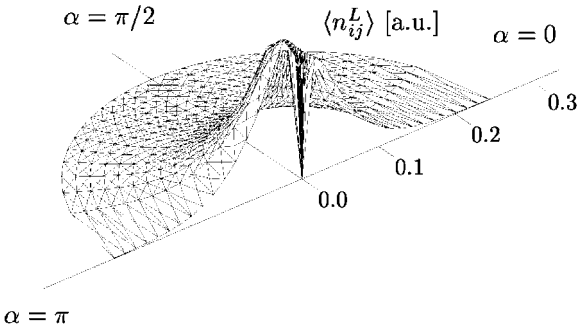

Figure 5. The electron densities $\langle n_{ij}^L \rangle$ versus the cells $\mathcal{C}_{ij}^L$ in the L valley, evaluated at $t = 8$ ps after the onset of the electric pulse with $E = 10\,\mathrm{kV\,cm^{-1}}$.

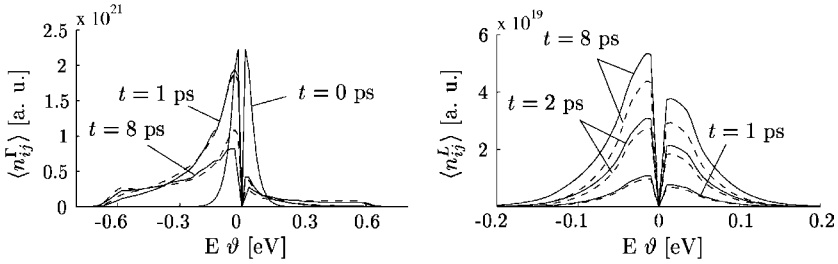

Figure 6. Cuts of electron densities $\langle n_{ij}^\Gamma \rangle$ and $\langle n_{ij}^L \rangle$ in the Γ and L valleys in the direction of the electric field versus the product of energy and cosine of the polar angle, $E\vartheta$, at several times after the beginning of the electric field pulse with $E = 10\,\mathrm{kV\,cm^{-1}}$. The solid lines refer to calculations taking into account non-equilibrium phonons, and the dashed lines refer to those assuming phonons to be at thermal equilibrium.

deviations of the results from the equilibrium distribution without an external electric field are small.

Finally, figure 6 illustrates cuts of the polar diagram representations of electron densities $\langle n_{ij}^\Gamma \rangle$ and $\langle n_{ij}^L \rangle$ in the Γ and L valleys in the direction of the electric field versus the product of energy and cosine of the polar angle, $E\vartheta$, at several times after the beginning of the electric field pulse with $E = 10\,\mathrm{kV\,cm^{-1}}$. Here, we compare the results obtained by taking into account hot electrons with those obtained assuming phonons to be in thermal equilibrium. The differences between the results lead to significantly different results for macroscopic quantities such as valley population, drift velocity and electron energy for calculations with and without hot phonons, as discussed in section 4.4. The detailed explanation of the physical effects which cause these differences is given in [4].

4.3. Phonon distribution function

The dynamics of the LO phonon distribution function is discussed in this section. Figure 7(*a*) illustrates the LO phonon densities $\langle r_{xy} \rangle$ in the cells $\mathcal{D}_{xy}$ at $t = 8$ ps after the onset of the electric pulse with $E = 10\,\mathrm{kV\,cm^{-1}}$. Here we find that the phonon density is undisturbed at low and high moduli of the wave vector, while it is enlarged for immediate q. Additionally, an asymmetry of the $\langle r_{xy} \rangle$ is observed, which corresponds to the asymmetry of the electron distribution in the Γ valley.

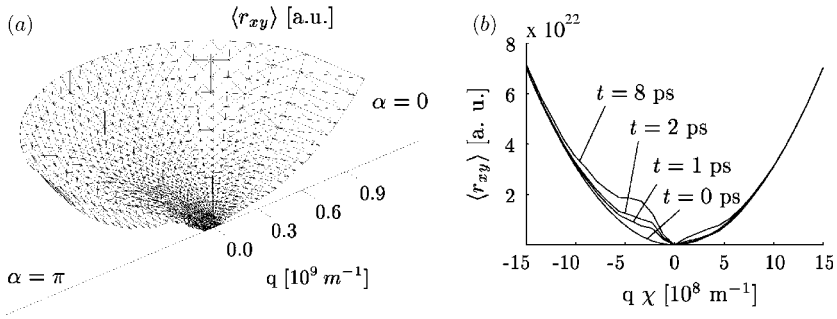

Figure 7. The LO phonon densities $\langle r_{xy}\rangle$ in the cells $\mathcal{D}_{xy}$ at $t = 8$ ps after the onset of the electric pulse (a) and cuts of the LO phonon densities $\langle r_{xy}\rangle$ in the direction of the electric field versus the z-component of the wave vector $q\chi$ at several times after the onset of the field pulse (b) with $E = 10\,\mathrm{kV\,cm^{-1}}$.

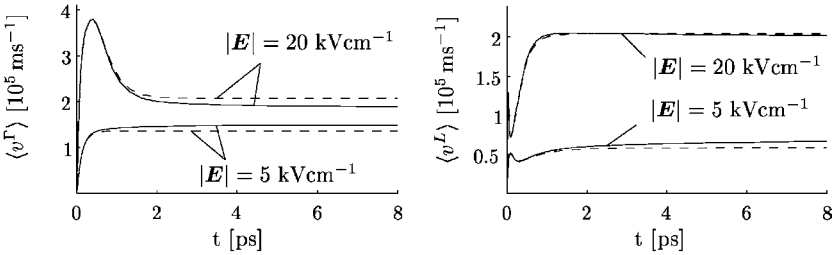

Figure 8. Average drift velocity $\langle v^{\Gamma}\rangle$ and $\langle v^{L}\rangle$ in the Γ and L valleys in the direction of the electric field versus the time t and the reported electric field. The solid lines refer to calculations taking into account non-equilibrium phonons, and the dashed lines refer to those assuming phonons to be at thermal equilibrium.

In figure 7(b), cuts of the LO phonon densities $\langle r_{xy}\rangle$ in the direction of the electric field versus the z-component of the wave vector $q\chi$ at several times after the beginning of the electric field pulse with $E = 10\,\mathrm{kV\,cm^{-1}}$ are displayed. The physical background, how the amplified reabsorption of the hot phonons affects the EDF, is found in [4].

4.4. Transport parameters

To investigate the effect of non-equilibrium phonons on transport parameters in the transient regime, we compare the drift velocities and energies of electrons in the Γ and L valleys as functions of time obtained with phonons at thermal equilibrium to those obtained by taking into account phonon disturbance.

Figure 8 reports the results for the drift velocity in the Γ and L valleys for electric fields of 5 and 20 $\mathrm{kV\,cm^{-1}}$. For times $t \leqslant 0.4$ ps, there is practically no difference between the drift velocities obtained with and without hot phonons. Thereafter, a modification of the temporal evolution of these quantities is observed, which finally leads to a significant difference between the values for the final stationary drift velocities. In figure 9, we display the average electron energy $\langle v^{\Gamma}\rangle$ and $\langle v^{L}\rangle$ in the Γ and L valleys versus time t for electric field strengths of $E = 5\,\mathrm{kV\,cm^{-1}}$ and $E = 20\,\mathrm{kV\,cm^{-1}}$. Here again, we find that hot phonons are responsible for a notable modification of the values of the final electron energy. Consequently, we state

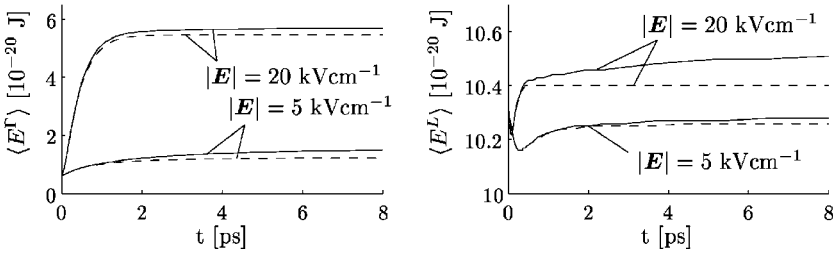

Figure 9. Average electron energy $\langle E^{\Gamma} \rangle$ and $\langle E^{L} \rangle$ in the Γ and L valleys versus the time t and the reported electric field. The solid lines refer to calculations taking into account non-equilibrium phonons, and the dashed lines refer to those assuming phonons to be at thermal equilibrium.

that in the cases of high donor densities, hot-phonon effects cannot be neglected in an accurate description of the transport parameters in polar semiconductors.

5. Conclusion

We present a multigroup model for the Boltzmann transport equations governing the evolution of the coupled electron–phonon system in polar semiconductors. Special effort is invested for the proper formulations of the force term and the POP interaction terms. In addition, expressions for handling all the other relevant scattering mechanisms are deduced.

Our method is used to study the transient transport regime in response to a step-like dc electric field pulse. This rather simple physical situation is chosen, because we intend to apply our model to an already carefully investigated problem, which allows us to prove its validity and applicability. In table 3, the dependence of the computation time on the applied electric field strength and the demanded relative accuracy is presented. The comparison of our model with the stationary iterative method [3], the matrix method [4] and Monte Carlo calculations [18] shows that the differences between the results obtained with the help of these methods are negligible.

Several figures illustrate the temporal evolution of the electron distribution functions in the Γ and L valleys and the LO phonon distribution function. Additionally, the dependence of some macroscopic quantities on time from the onset of the electric field pulse is discussed.

Regarding the numerical properties of our model, we find two advantages in comparison to other mesoscopic methods: (i) the collision coefficients are found to be analytical expressions as shown in the appendix and (ii) the evaluation of the collision terms is performed in a very efficient way, even the non-linear POP interaction term is simply given as the product of the unknowns with a constant collision coefficient. Consequently, our method combines high numerical accuracy and affordable computation time.

Therefore, we regard our method as a very powerful tool for investigating the coupled electron–phonon system of polar semiconductors, whose accurate description is essential for deeper understanding of modern highly integrated semiconductor devices.

Acknowledgment

This work was supported by the Fond zur Förderung der wissenschaftlichen Forschung, Vienna, under contract number P14669-TPH.

Appendix. The evaluation of the collision coefficients

To demonstrate how to proceed, we evaluate the collision coefficient $\langle \mathcal{A}^{\nu,xy}_{\mathrm{POP},ab}\rangle_{ij}$ in this section. Therefore, we consider equation (31*b*). First of all, we recognize that

$$\begin{aligned}|\boldsymbol{k}'-\boldsymbol{k}| &= \{k^2+k'^2-2kk'[[(1-\vartheta^2)(1-\vartheta'^2)]^{\frac{1}{2}}\cos\varphi'+\vartheta\vartheta']\}^{\frac{1}{2}}\\ (\boldsymbol{k}'-\boldsymbol{k})\cdot\boldsymbol{e}_z &= k'\vartheta'-k\vartheta\end{aligned} \tag{A.1}$$

as can easily be verified in the polar representation of $\boldsymbol{k}$ and $\boldsymbol{k}'$, setting $\boldsymbol{k}$ to the (x, z) plane. By representing the integration with respect to $\boldsymbol{k}'$ in spherical coordinates, we find, skipping the valley index ν,

$$\begin{aligned}\langle \mathcal{A}^{xy}_{\mathrm{POP},ab}\rangle_{ij} &= 8\pi^3 V\frac{K_{\mathrm{POP}}}{q_x^3}\int_{I_i^{\mathcal{E}}}\mathrm{d}E\int_{I_j^{\Theta}}\mathrm{d}\vartheta\int_{I_a^{\mathcal{E}}}\mathrm{d}E'Z(E')\int_{I_b^{\Theta}}\mathrm{d}\vartheta'\int_0^{2\pi}\mathrm{d}\varphi'\delta(E-E_i)\\ &\times\delta\{\{k(E)^2+k(E')^2-2k(E)k(E')[[(1-\vartheta^2)(1-\vartheta'^2)]^{\frac{1}{2}}\cos\varphi'+\vartheta\vartheta']\}^{\frac{1}{2}}-q_x\}\\ &\times\delta(\vartheta-\vartheta_j)\delta[(k(E')\vartheta'-k(E)\vartheta)-q_x\chi_y]\delta(E'-E+\hbar\omega_{\mathrm{LO}}).\end{aligned} \tag{A.2}$$

Carrying out the integrations with respect to E, E' and ϑ yields

$$\begin{aligned}\langle \mathcal{A}^{xy}_{\mathrm{POP},ab}\rangle_{ij} &= 8\pi^3 V\frac{K_{\mathrm{POP}}}{q_x^3}Z(E_i+\hbar\omega_{\mathrm{LO}})H[\mathcal{E}_a-(E_i+\hbar\omega_{\mathrm{LO}})]H(E_i+\hbar\omega_{\mathrm{LO}}-\mathcal{E}_{a-1})\\ &\times\int_{I_b^{\Theta}}\mathrm{d}\vartheta'\int_0^{2\pi}\mathrm{d}\varphi'\delta[k(E_i+\hbar\omega_{\mathrm{LO}})\vartheta'-k(E_i)\vartheta_j-q_x\chi_y]\delta\big\{\big\{k(E_i)^2+k(E_i+\hbar\omega_{\mathrm{LO}})^2\\ &-2k(E_i)k(E_i+\hbar\omega_{\mathrm{LO}})\big[\big[\big(1-\vartheta_j^2\big)(1-\vartheta'^2)\big]^{\frac{1}{2}}\cos\varphi'+\vartheta_j\vartheta'\big]\big\}^{\frac{1}{2}}-q_x\big\}.\end{aligned} \tag{A.3}$$

The symbol H denotes the Heaviside step function. By rewriting the Dirac distribution

$$\delta(|\boldsymbol{k}'-\boldsymbol{k}|-q_x)=\frac{2q_x\delta\big[\varphi'-\arccos\mathcal{N}^x_{ij}(\vartheta')\big]}{\big|k(E_i)k(E_i+\hbar\omega_{\mathrm{LO}})\big[\big(1-\vartheta_j^2\big)(1-\vartheta'^2)\big(1-\mathcal{N}^x_{ij}(\vartheta')^2\big)\big]^{\frac{1}{2}}\big|} \tag{A.4}$$

where

$$\mathcal{N}^x_{ij}(\vartheta')=\frac{k(E_i)^2+k(E_i+\hbar\omega_{\mathrm{LO}})^2-q_x^2-2k(E_i)k(E_i+\hbar\omega_{\mathrm{LO}})\vartheta_j\vartheta'}{2k(E_i)k(E_i+\hbar\omega_{\mathrm{LO}})\big[\big(1-\vartheta_j^2\big)(1-\vartheta'^2)\big]^{\frac{1}{2}}} \tag{A.5}$$

we achieve

$$\begin{aligned}\langle \mathcal{A}^{xy}_{\mathrm{POP},ab}\rangle_{ij} &= 16\pi^3 V\frac{K_{\mathrm{POP}}}{q_x^2}Z(E_i+\hbar\omega_{\mathrm{LO}})H[\mathcal{E}_a-(E_i+\hbar\omega_{\mathrm{LO}})]H(E_i+\hbar\omega_{\mathrm{LO}}-\mathcal{E}_{a-1})\\ &\times\int_{I_b^{\Theta}}\mathrm{d}\vartheta'\frac{H\big[\arccos\mathcal{N}^x_{ij}(\vartheta')\big]\delta\left[k(E_i+\hbar\omega_{\mathrm{LO}})\vartheta'-k(E_i)\vartheta_j-q_x\chi_y\right]}{\big|k(E_i)k(E_i+\hbar\omega_{\mathrm{LO}})\big[\big(1-\vartheta_j^2\big)(1-\vartheta'^2)\big(1-\mathcal{N}^x_{ij}(\vartheta')^2\big)\big]^{\frac{1}{2}}\big|}.\end{aligned} \tag{A.6}$$

Finally, we find

$$\begin{aligned}\langle \mathcal{A}^{xy}_{\mathrm{POP},ab}\rangle_{ij} &= 16\pi^3 V\frac{K_{\mathrm{POP}}}{q_x^2}\frac{Z(E_i+\hbar\omega_{\mathrm{LO}})}{k(E_i)k(E_i+\hbar\omega_{\mathrm{LO}})}H\big[\arccos\hat{\mathcal{N}}^{xy}_{ij}\big]H[\mathcal{E}_a-(E_i+\hbar\omega_{\mathrm{LO}})]\\ &\times H(E_i+\hbar\omega_{\mathrm{LO}}-\mathcal{E}_{a-1})H\left[\Theta_b-\frac{k(E_i)\vartheta_j+q_x\chi_y}{k(E_i+\hbar\omega_{\mathrm{LO}})}\right]H\left[\frac{k(E_i)\vartheta_j+q_x\chi_y}{k(E_i+\hbar\omega_{\mathrm{LO}})}-\Theta_{b-1}\right]\\ &\times\big\{\big(1-\vartheta_j^2\big)[k(E_i+\hbar\omega_{\mathrm{LO}})^2-(k(E_i)\vartheta_j+q_x\chi_y)^2]\big(1-\hat{\mathcal{N}}^{xy2}_{ij}\big)\big\}^{-\frac{1}{2}}\end{aligned} \tag{A.7}$$

with

$$\hat{\mathcal{N}}_{ij}^{xy} = \mathcal{N}_{ij}^{x}\left(\frac{k(E_i)\vartheta_j + q_x\chi_y}{k(E_i + \hbar\omega_{\mathrm{LO}})}\right). \tag{A.8}$$

As the most important result of this section, we note that the collision coefficient $\left\langle \mathcal{A}_{\mathrm{POP},ab}^{xy}\right\rangle_{ij}$ as well as the other POP interaction coefficients can be calculated analytically.

References

[1] Markovic P, Ringhofer C and Schmeiser C 1990 *Semiconductor Equations* (Vienna: Springer)

[2] Ferry D K 1991 *Semiconductors* (New York: Macmillan)

[3] Vaissiere J C, Nougier J P, Fadel M, Hlou L and Kocevar P 1992 Numerical solution of coupled steady state hot-phonon–hot-electron Boltzmann equations in InP *Phys. Rev.* B **46** 13082–99

[4] Vaissiere J C, Nougier J P, Varani L, Houlet P, Hlou L, Reggiani L and Kocevar P 1996 Nonequilibrium phonon effects on the transient high-field transport regime in InP *Phys. Rev.* B **53** 9886–94

[5] Fatemi E and Odeh F 1993 Upwind finite difference solution of Boltzmann equation applied to electron transport in semiconductor devices *J. Comput. Phys.* **108** 209–17

[6] Majorana A and Pidatella R M 2001 A finite difference scheme solving the Boltzmann–Poisson system for semiconductor devices *J. Comput. Phys.* **174** 649–68

[7] Carrillo J A, Gamba I M, Majorana A and Shu C-W 2003 A WENO-solver for the transients of Boltzmann–Poisson system for semiconductor devices: performance and comparisons with Monte Carlo methods *J. Comput. Phys.* **184** 498–525

[8] Ringhofer C 1997 Computational methods for semiclassical and quantum transport in semiconductor devices *Acta Num.* **3** 485–521

[9] Ringhofer C 2000 Space-time discretization methods for series expansion solutions of the Boltzmann equation for semiconductors *SIAM J. Numer. Anal.* **38** 442–65

[10] Ringhofer C, Schmeiser C and Zwirchmayer A 2001 Moment methods for the semiconductor Boltzmann equation in bounded position domains *SIAM J. Numer. Anal.* **39** 1078–95

[11] Lapidus L and Pinder G F 1982 *Numerical Solution of Partial Differential Equations in Science and Engineering* (New York: Wiley)

[12] Caraffini G L, Ganapol B and Spiga G A 1995 Multigroup approach to the non-linear extended Boltzmann equation *Nuovo Cimento* **17** 129–42

[13] Galler M, Rossani A and Schürrer F 2003 A variable multigroup approach to the nonlinear Boltzmann equation based on the method of weighted residuals *Rarefied Gas Dynamics* ed A D Ketsdever and E P Muntz (New York: Springer) pp 43–50

[14] Galler M, Schürrer F and Rossani A 2002 Moment equations of a conservative multigroup approximation to the nonlinear 3D Boltzmann equation *Trans. Theor. Stat. Phys.* at press

[15] Lundstrom M 2000 *Fundamentals of Carrier Transport* (Cambridge: Cambridge University Press)

[16] Ziman J M 2001 *Electrons and Phonons* (Oxford: Clarendon)

[17] Ertler C and Schürrer F 2003 A multicell matrix solution to the Boltzmann equation applied to the anisotropic electron transport in silicon *J. Phys. A: Math. Gen.* **36** 8759–74

[18] Maloney T J and Frey J 1976 Transient and steady-state electron transport properties of GaAs and InP *J. Appl. Phys.* **48** 781–7